The Astrophysical Journal, 804:28 (10pp), 2015 May 1 doi:10.1088/0004-637X/804/1/28
© 2015. The American Astronomical Society. All rights reserved.

GALEX DETECTION OF SHOCK BREAKOUT IN TYPE IIP SUPERNOVA PS1-13arp: IMPLICATIONS FOR THE PROGENITOR STAR WIND

S. Gezari[1], D. O. Jones[2], N. E. Sanders[3], A. M. Soderberg[3], T. Hung[1], S. Heinis[1], S. J. Smartt[4], A. Rest[5], D. Scolnic[6], R. Chornock[7], E. Berger[3], R. J. Foley[8,9], M. E. Huber[10], P. Price[11], C. W. Stubbs[3,12], A. G. Riess[2], R. P. Kirshner[3,12], K. Smith[4], W. M. Wood-Vasey[13], D. Schiminovich[14], D. C. Martin[15], W. S. Burgett[16], K. C. Chambers[10], H. Flewelling[10], N. Kaiser[10], J. L. Tonry[10], and R. Wainscoat[10]

[1] Department of Astronomy, University of Maryland, Stadium Drive, College Park, MD 20742–2421, USA; suvi@astro.umd.edu
[2] Department of Physics and Astronomy, Johns Hopkins University, 3400 North Charles Street, Baltimore, Maryland 21218, USA
[3] Harvard-Smithsonian Center for Astrophysics, 60 Garden Street, Cambridge, Massachusetts 02138, USA
[4] Astrophysics Research Centre, School of Mathematics and Physics, Queen's University Belfast, Belfast BT7 1NN, UK
[5] Space Telescope Science Institute, 3700 San Martin Drive, Baltimore, Maryland 21218, USA
[6] Kavli Institute for Cosmological Physics, University of Chicago, 5640 South Ellis Avenue, Chicago, IL 60637, USA
[7] Ohio University, 1 Ohio University, Athens, OH 45701, USA
[8] Astronomy Department, University of Illinois at Urbana-Champaign, 1002 West Green Street, Urbana, IL 61801, USA
[9] Department of Physics, University of Illinois Urbana-Champaign, 1110 West Green Street, Urbana, IL 61801 USA
[10] Institute for Astronomy, University of Hawaii, 2680 Woodlawn Drive, Honolulu, Hawaii 96822, USA
[11] Department of Astrophysical Sciences, Princeton University, 4 Ivy Lane, Princeton, NJ, 08544, USA
[12] Department of Physics, Harvard University, USA
[13] Pittsburgh Particle Physics, Astrophysics, and Cosmology Center, Department of Physics and Astronomy, University of Pittsburgh, 3941 O'Hara Street, Pittsburgh, Pennsylvania, PA 15260, USA
[14] Department of Astronomy, Columbia University, 550 West 120th Street, New York, NY 10027, USA
[15] Astronomy Department, California Institute of Technology, MC 249-17, 1200 East California Boulevard, Pasadena, CA 91125, USA
[16] GMTO Corporation, 251 S. Lake Avenue, Suite 300, Pasadena, CA 91101, USA
Received 2015 January 26; accepted 2015 February 23; published 2015 April 27

ABSTRACT

We present the *GALEX* detection of a UV burst at the time of explosion of an optically normal supernova (SN) IIP (PS1-13arp) from the Pan-STARRS1 survey at $z = 0.1665$. The temperature and luminosity of the UV burst match the theoretical predictions for shock breakout in a red supergiant (RSG), but with a duration a factor of ∼50 longer than expected. We compare the NUV light curve of PS1-13arp to previous *GALEX* detections of SNe IIP and find clear distinctions that indicate that the UV emission is powered by shock breakout, and not by the subsequent cooling envelope emission previously detected in these systems. We interpret the ∼1 day duration of the UV signal with a shock breakout in the wind of an RSG with a pre-explosion mass-loss rate of $\sim 10^{-3}\ M_{\odot}\ \mathrm{yr}^{-1}$. This mass-loss rate is enough to prolong the duration of the shock breakout signal, but not enough to produce an excess in the optical plateau light curve or narrow emission lines powered by circumstellar interaction. This detection of non-standard, potentially episodic high mass loss in an RSG SN progenitor has favorable consequences for the prospects of future wide-field UV surveys to detect shock breakout directly in these systems, and provide a sensitive probe of the pre-explosion conditions of SN progenitors.

Key words: supernovae: individual (PS1-13arp) – surveys – ultraviolet: general

1. INTRODUCTION

The first electromagnetic signature of a core-collapse supernova (SN) is expected to occur when the explosion shock wave accelerates through the stellar envelope and the radiation from the shock escapes and "breaks out" of the stellar surface (Falk 1978; Klein & Chevalier 1978). This radiative precursor to the SN explosion is expected to be the most luminous phase of an SN, and yet it is the least well observed. This is because the associated burst of radiation is brief (1–1000 s) and hot ($\sim 10^5 - 10^6$ K; Klein & Chevalier 1978; Ensman & Burrows 1992; Blinnikov et al. 2002), and *precedes* the optically bright phase during which SNe are typically discovered.

These obstacles to discovery were surmounted with a bit of luck in a pointed X-ray observation of a galaxy in which an SN Ibc fortuitously exploded, and a several hundred second X-ray flash was detected (Soderberg et al. 2008; Modjaz et al. 2009) with a duration and spectral shape consistent with shock breakout into the thick wind of a Wolf–Rayet (WR) star progenitor (Balberg & Loeb 2011; Svirski & Nakar 2014). The presence of a thick wind is expected for a WR star, but it was also an important factor in stretching the shock breakout timescale long enough (a factor of 100 longer than expected for shock breakout through the stellar surface) to be easily detectable. In fact, there have been reports of shock breakout detections in SNe II on a timescale of hours to several days (Schawinski et al. 2008; Ofek et al. 2010, 2013; Drout et al. 2014), which require an unusual amount of circumstellar material in order to explain the timing of the events, either in the form of an extended stellar envelope inconsistent with stellar evolution models (Schawinski et al. 2008), or a vigorous, episodic mass-loss rate of $\approx 0.1\ M_{\odot}\ \mathrm{yr}^{-1}$ (Ofek et al. 2010; Drout et al. 2014).

A few of the earliest optical discoveries of core-collapse SNe have caught the decline of the "cooling envelope phase" following shock breakout (Hamuy et al. 1988; Stritzinger et al. 2002; Dessart et al. 2008). Observing the *rise* to the peak of the cooling envelope emission is more desirable because it puts direct constraints on the radius of the progenitor star (Nakar & Sari 2010; Rabinak & Waxman 2011). This thermal emission from the expanding shock-heated ejecta lasts only minutes in the soft X-rays, but peaks in the UV from hours up

to a couple days after shock breakout (Nakar & Sari 2010). By the time the thermal emission peaks in the optical, other radiative processes dominate, i.e., radioactivity (and hydrogen recombination in SNe II). The timescales of the UV peak are more accessible to SN surveys; however, they still require observing the SN in the UV *before* it brightens in the optical, which can be days later. With *GALEX* we have attempted to circumvent this problem by coordinating wide-field monitoring in the UV with ground-based monitoring in the optical.

The large radii of red supergiant (RSG) stars yield longer timescales and larger luminosities during shock breakout and its immediate aftermath, making them appealing for observational searches. Stellar evolution calculations predict that RSG stars will explode as SNe IIP (Heger et al. 2003), and SNe IIP have been directly linked with RSG progenitors from pre-explosion imaging (Smartt et al. 2009). Indeed, the first early UV detections of SNe were of two SNe IIP, which were discovered serendipitously from overlap between the *GALEX* Deep Imaging Survey and the Canada–France–Hawaii Telescope (CFHT) Supernova Legacy Survey (Gezari et al. 2008; Schawinski et al. 2008).

The first planned UV and optical joint survey effort, the *GALEX* Time Domain Survey (Gezari et al. 2013) in the NUV, was coordinated with the optical Pan-STARRS1 Medium Deep Survey (PS1 MDS) and yielded an early detection of the rise to the peak of UV emission from an SN IIP at $z = 0.0862$ with a cadence of two days. The early UV peak was well fitted by cooling envelope emission from the explosion of an RSG with $R = 700 \pm 200\,R_{\odot}$ (Gezari et al. 2010). While the *GALEX* observations caught the rise to the peak of the cooling envelope emission, the shock breakout itself was not resolved by the relatively coarse time sampling of the observations compared to the expected shock breakout duration (<1 hr). Ganot et al. (2014) present a shallower, wide-field joint NUV *GALEX* and optical Palomar Transient Factory (PTF) survey that detected seven core-collapse SNe in the UV with a three-day cadence. Their observed detection rate is consistent with core-collapse SN rates combined with a fiducial model for cooling envelope emission from RSG stars. However, again their cadence was not sufficient to catch the short-lived shock breakout signal.

Here we present the results from a high-cadence monitoring program with *GALEX* that increased the time sampling of the *GALEX* Time Domain Survey and *GALEX*/PTF survey by a factor of two and three, respectively, and has yielded the first potential detection of the elusive shock breakout phase in an SN IIP, albeit with the requirement that the shock breakout occurred outside the progenitor's surface, in its circumstellar wind. The paper is organized as follows. In Section 2 we describe the *GALEX* and PS1 MDS observations and Gemini spectroscopy; in Section 3 we compare the UV/optical light curve of PS1-13arp to previous early observations of SNe IIP; in Section 4 we compare the observed UV burst to models for shock breakout from the surface of a star, cooling envelope emission, and shock breakout into a wind; and in Section 5 we conclude with our favored model of shock breakout of an RSG with a pre-explosion mass-loss rate of $\approx 10^{-3}\,M_{\odot}$ yr^{-1}.

2. OBSERVATIONS

2.1. Pan-STARRS1 Medium Deep Survey

The Pan-STARRS1 system is a high-etendue wide-field imaging system, designed for dedicated survey observations. The system is installed on the peak of Haleakala on the island of Maui in the Hawaiian island chain. A description of the Pan-STARRS1 system, both hardware and software, is provided by Kaiser et al. (2010). The Pan-STARRS1 optical design (Hodapp et al. 2004) uses a 1.8 m diameter *f*/4.4 primary mirror and a 0.9 m secondary, and a 3.3 deg diameter field of view. The Pan-STARRS1 imager (Tonry & Onaka 2009) comprises a total of sixty 4800 × 4800 pixel detectors, with 10 μm pixels that subtend 0.258 arcsec.

The PS1 observations were obtained through a set of five broadband filters, which we have designated as $g_{\rm P1}$, $r_{\rm P1}$, $i_{\rm P1}$, $z_{\rm P1}$, and $y_{\rm P1}$. Although the filter system for Pan-STARRS1 has much in common with that used in previous surveys, such as SDSS (Abazajian et al. 2009), there are important differences. Further information on the passband shapes is described in Stubbs et al. (2010). Photometry is in the "natural" Pan-STARRS1 system, $m = -2.5\log(flux) + m'$, with a single zero-point adjustment m′ made in each band to conform to the AB magnitude scale (Tonry et al. 2012).

Images obtained by the Pan-STARRS1 system are processed through the Image Processing Pipeline (IPP; Magnier 2006) on a computer cluster at the Maui High Performance Computer Center. The pipeline runs the images through a succession of stages, including flat-fielding ("de-trending"), a flux-conserving warping to a sky-based image plane (with a plate scale of 0.25 arcsec pixel^{-1}), masking and artifact removal, and object detection and photometry. Mask and variance arrays are carried forward at each stage of the IPP processing. Photometric and astrometric measurements performed by the IPP system are described in Magnier (2007) and Magnier et al. (2008), respectively.

PS1 has two extragalactic survey modes: the 3π survey observes the entire sky above a declination of −30 deg in five bands with a sparse cadence (a few epochs per month per filter), and the MDS is a deeper survey of 10 fields distributed across the sky in five filters with a daily cadence. This paper uses images and photometry from the PS1 MDS. Observations of three to five MD fields are taken each night and the filters are cycled through in the following pattern: $g_{\rm P1}$ and $r_{\rm P1}$ in the same night (dark time), followed by $i_{\rm P1}$ and $z_{\rm P1}$ on the subsequent second and third nights, respectively. Around full moon only $y_{\rm P1}$ data are taken. A nightly stacked image is created using a variance-weighted scheme from eight dithered exposures, allowing for the removal of defects like cosmic rays and satellite streaks, and resulting in a 5σ depth of ∼23 mag in the $g_{\rm P1}$, $r_{\rm P1}$, $i_{\rm P1}$, and $z_{\rm P1}$ bands, and ∼22 mag in the $y_{\rm P1}$ band in the AB system.

The nightly MD stacked images are processed through a frame-subtraction analysis using the *photpipe* pipeline (Rest et al. 2005), and significant excursions in the difference images are detected using a modified version of DoPHOT (Schechter et al. 1993). Reference templates are constructed for the MD fields from two epochs obtained at the beginning of the observing season. Spectroscopically confirmed SNe are later reprocessed using deep template images, constructed from all nightly stacks with good seeing in the seasons that the SN did not explode, with the routine *transphot* (Rest et al. 2014), which implements the HOTPANTS image differencing algorithm (Becker et al. 2004), then point-spread function (PSF) photometry is applied using DAOPHOT (Stetson 1987). The weighted average position of the SN is calculated, and forced photometry is then applied in every difference image at that

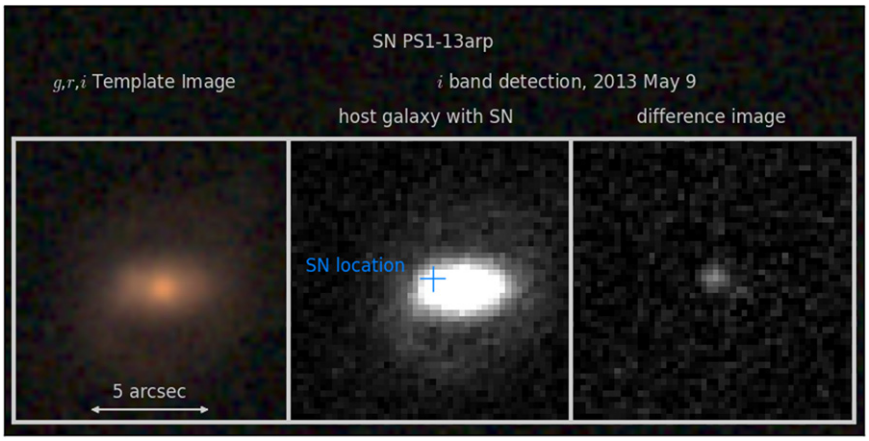

Figure 1. PS1 deep g_{P1}, r_{P1}, i_{P1} reference template (left), *i*-band image on UT 2013 May 9 (middle), and *i*-band difference image (right). The position of PS1-13arp in the host galaxy is marked with a blue cross.

position. The PS1 MDS SN search has yielded hundreds of spectroscopically confirmed SNe, including SNe Ia for cosmology studies (Rest et al. 2014), core-collapse SNe, including 76 SNe IIP (Sanders et al. 2014), as well as several rare, superluminous SNe at high redshift (Chomiuk et al. 2011; Berger et al. 2012; Lunnan et al. 2013).

2.2. GALEX High-cadence Time Domain Survey

We conducted an extended survey with *GALEX* in the NUV during 2012 December through 2013 April of four PS1 MD fields, in order to perform a high-cadence (1 day) time domain survey and to complete *GALEX* coverage started with the *GALEX* Time Domain Survey (Gezari et al. 2013) for 9 out of the 10 PS1 MD fields. The FUV detector on *GALEX* was no longer operational after 2009 May. The one-day cadence of the *GALEX* observations was chosen to better probe the cooling envelope emission of RSG stars, which has a characteristic timescale of two days (Nakar & Sari 2010; Rabinak & Waxman 2011) and was just barely resolved by the two-day cadence of the *GALEX* Time Domain Survey for the SN IIP 2010aq (Gezari et al. 2010). The exposure times for each *GALEX* visit averaged 1.1 ks, resulting in a 3σ depth of 23.5 mag in the NUV in the AB system. Here we present the joint *GALEX* and PS1 discovery of SN IIP PS1-13arp, for which we catch the onset of a luminous UV burst with *GALEX* that precedes its standard optical behavior observed by PS1.

2.3. Imaging and Spectroscopy of PS1-13arp

PS1-13arp was identified as an optical transient in the PS1 field MD06 by *photpipe* on UT 2013 April 26 at R.A. 12:18:25.108, decl. +46:37:01.30 (J2000), with a spatial offset of 1.577 arcsec east and 0.275 arcsec north of its host galaxy (SDSS J121824.98+463700.5). Figure 1 shows the PS1 difference image detection in the *i*band, as well as a color image of the deep reference template with only the host galaxy flux. The SN was also detected as a variable source by *GALEX* during monitoring of the field PS_NGC4258_MOS107 at the 8.3σ level on UT 2013 April 15. The host galaxy is detected in the NUV and measured from the four epochs before the SN is detected by the *GALEX* pipeline to have NUV $= 21.20 \pm 0.05$ mag, measured from a 6 arcsec radius circular aperture and including a correction for the total enclosed energy of −0.23 mag (Morrissey et al. 2007). Table 1 gives the SN photometry from *GALEX* and PS1.

We obtained spectroscopy of the UV/optical transient with Gemini/GMOS on UT 2013 May 4. We obtained three exposures with a 1.0 arcsec slit and an R400 grating of 1200 s each, resulting in a spectral resolution of ∼4 Å with a dither along the slit and a change in the grating central wavelength in order to avoid bad columns and to cover the gap in wavelength coverage for the grating. The spectrum was overscan-corrected, bias-subtracted, flat-fielded, wavelength-calibrated, and flux-calibrated using standard IRAF routines. Observations of a standard star (Feige 34) were used for flux calibration and corrections for telluric absorption. The 2D spectrum displays strong, spatially extended emission lines (Hα, [N II] $\lambda\lambda$6583, 6548, [S II]$\lambda\lambda$6716, 6731) indicative of star formation in the host galaxy, from which we measure a redshift of $z = 0.1665 \pm 0.001$.

We fitted the rest-frame host galaxy broadband spectral energy distribution (SED) from *GALEX* FUV and NUV (Martin et al. 2005), PS1 g_{P1}, r_{P1}, i_{P1}, z_{P1}, y_{P1} deep stacks with *u*-band coverage from CFHT (S. Heinis et al. 2015, in preparation), and infrared from *WISE* at 3.4 and 4.6 μm (Wright et al. 2010) with the code CIGALE (Noll et al. 2009) using version v0.3, implemented in Python. CIGALE combines a UV–optical stellar SED with a dust component emitting in the infrared, and ensures a full energy balance between the dust absorbed stellar emission and its re-emission in the IR. The fit requires both an old stellar population with an exponentially declining star formation rate with $\tau = 6.7 \pm 2$ Gyr as well as a recent stellar population with a moderate star formation rate of $3.6 \pm 1.2\ M_{\odot}\ \mathrm{yr}^{-1}$, with a total stellar mass of $\log\left(M/M_{\odot}\right) = 10.4 \pm 0.1$. Note that this mass is consistent with the gas-phase metallicity that we estimate from the ratio of the strong nebular emission lines in the host galaxy spectrum. We measure $\log([\mathrm{NII}]\lambda6584/H\alpha) = -0.37 \pm 0.06$, which corresponds to a metallicity of $\log(\mathrm{O/H}) + 12 \approx 9$ (Kewley & Dopita 2002), and is in good agreement with the mass–metallicity relation for star-forming galaxies (Tremonti et al. 2004).

We extract a 1D SN spectrum by first extracting a 1D spectrum using a 5 pixel aperture centered on the SN (including SN and galaxy light), and then extract a 1D spectrum with an aperture centered on a region 5 pixels away from the SN center, with only galaxy light. We isolate the SN

Table 1
GALEX and PS1 Photometry

Filter	Date (MJD)	ϕ (days)[a]	mag[b]	1σ
NUV	56393.07	−2.9	<23.69	⋯
NUV	56394.03	−2.1	<23.70	⋯
NUV	56395.05	−1.2	<23.63	⋯
NUV	56396.02	−0.4	<23.65	⋯
NUV	56397.04	0.5	21.58	0.06
NUV	56398.00	1.3	21.60	0.06
NUV	56399.02	2.2	22.14	0.10
NUV	56399.98	3.0	22.40	0.07
NUV	56401.01	3.9	22.05	0.15
NUV	56401.96	4.7	23.35	0.12
g_{P1}	56325.60	−60.8	<23.16	⋯
g_{P1}	56328.60	−58.2	<23.57	⋯
g_{P1}	56331.60	−55.6	<23.90	⋯
g_{P1}	56336.60	−51.3	<23.84	⋯
g_{P1}	56354.60	−35.9	<23.25	⋯
g_{P1}	56357.60	−33.3	<23.82	⋯
g_{P1}	56384.50	−10.3	<23.35	⋯
g_{P1}	56387.50	−7.7	<23.55	⋯
g_{P1}	56390.40	−5.2	<23.48	⋯
g_{P1}	56398.50	1.7	22.34	0.13
g_{P1}	56401.30	4.1	22.41	0.23
g_{P1}	56416.40	17.1	22.69	0.18
g_{P1}	56421.30	21.3	22.98	0.17
g_{P1}	56427.30	26.4	23.22	0.26
g_{P1}	56430.40	29.1	24.44	1.13
g_{P1}	56443.30	40.1	23.41	0.22
g_{P1}	56451.30	47.0	24.03	0.52
g_{P1}	56460.30	54.7	24.09	0.46
g_{P1}	56478.30	70.1	26.19	3.25
r_{P1}	56325.60	−60.8	<23.18	⋯
r_{P1}	56328.60	−58.2	<23.37	⋯
r_{P1}	56331.60	−55.6	<23.40	⋯
r_{P1}	56332.60	−54.8	<23.51	⋯
r_{P1}	56336.60	−51.3	<23.41	⋯
r_{P1}	56354.60	−35.9	<23.17	⋯
r_{P1}	56357.60	−33.3	<23.24	⋯
r_{P1}	56371.50	−21.4	<23.31	⋯
r_{P1}	56384.50	−10.3	<23.26	⋯
r_{P1}	56387.50	−7.7	<23.14	⋯
r_{P1}	56390.40	−5.2	<23.05	⋯
r_{P1}	56398.50	1.7	23.12	0.34
r_{P1}	56401.30	4.1	22.71	0.22
r_{P1}	56416.40	17.1	22.48	0.19
r_{P1}	56420.40	20.5	22.43	0.14
r_{P1}	56427.30	26.4	22.36	0.16
r_{P1}	56430.40	29.1	22.61	0.21
r_{P1}	56443.30	40.1	23.08	0.32
r_{P1}	56450.30	46.1	24.65	1.86
r_{P1}	56460.30	54.7	23.16	0.30
r_{P1}	56478.30	70.1	23.14	0.34
i_{P1}	56323.60	−62.5	<22.79	⋯
i_{P1}	56326.60	−59.9	<23.21	⋯
i_{P1}	56332.60	−54.8	<23.34	⋯
i_{P1}	56334.50	−53.1	<23.22	⋯
i_{P1}	56337.60	−50.5	<23.29	⋯
i_{P1}	56352.50	−37.7	<22.78	⋯

Table 1
(Continued)

Filter	Date (MJD)	ϕ (days)[a]	mag[b]	1σ
i_{P1}	56355.50	−35.1	<23.29	⋯
i_{P1}	56358.60	−32.5	<23.15	⋯
i_{P1}	56369.40	−23.2	<23.05	⋯
i_{P1}	56388.50	−6.8	<22.96	⋯
i_{P1}	56391.40	−4.4	<23.16	⋯
i_{P1}	56393.30	−2.7	<23.23	⋯
i_{P1}	56396.50	0.0	<22.96	⋯
i_{P1}	56399.40	2.5	23.05	0.29
i_{P1}	56403.40	5.9	22.62	0.20
i_{P1}	56411.40	12.8	22.27	0.35
i_{P1}	56414.40	15.4	22.26	0.17
i_{P1}	56417.40	17.9	22.39	0.18
i_{P1}	56420.40	20.5	22.39	0.15
i_{P1}	56422.30	22.1	22.32	0.16
i_{P1}	56432.30	30.7	22.47	0.18
i_{P1}	56444.30	41.0	22.44	0.17
i_{P1}	56447.30	43.6	22.45	0.17
i_{P1}	56450.30	46.1	22.52	0.25
i_{P1}	56452.30	47.8	22.50	0.19
i_{P1}	56455.30	50.4	22.53	0.18
i_{P1}	56458.30	53.0	22.49	0.21
i_{P1}	56462.30	56.4	22.71	0.21
i_{P1}	56479.30	71.0	22.74	0.21
z_{P1}	56324.60	−61.6	<22.64	⋯
z_{P1}	56338.60	−49.6	<22.71	⋯
z_{P1}	56348.60	−41.1	<22.47	⋯
z_{P1}	56351.50	−38.6	<22.62	⋯
z_{P1}	56353.50	−36.9	<22.56	⋯
z_{P1}	56356.50	−34.3	<22.76	⋯
z_{P1}	56359.60	−31.6	<22.61	⋯
z_{P1}	56364.50	−27.4	<22.61	⋯
z_{P1}	56370.40	−22.4	<22.73	⋯
z_{P1}	56383.50	−11.1	<22.63	⋯
z_{P1}	56386.30	−8.7	<22.67	⋯
z_{P1}	56389.50	−6.0	<22.59	⋯
z_{P1}	56392.30	−3.6	<22.67	⋯
z_{P1}	56394.30	−1.9	<22.48	⋯
z_{P1}	56397.40	0.8	<22.59	⋯
z_{P1}	56400.40	3.4	23.17	0.63
z_{P1}	56402.30	5.0	22.11	0.27
z_{P1}	56404.30	6.7	22.40	0.29
z_{P1}	56410.40	11.9	22.60	0.36
z_{P1}	56412.40	13.6	22.48	0.32
z_{P1}	56415.40	16.2	22.29	0.25
z_{P1}	56421.40	21.4	22.51	0.30
z_{P1}	56423.40	23.1	22.10	0.22
z_{P1}	56429.30	28.1	22.32	0.27
z_{P1}	56451.30	47.0	22.42	0.30
z_{P1}	56453.30	48.7	22.95	0.64
z_{P1}	56456.30	51.3	22.31	0.27
z_{P1}	56459.30	53.8	22.55	0.31
z_{P1}	56461.30	55.6	22.61	0.36
z_{P1}	56463.30	57.3	22.66	0.35
z_{P1}	56480.30	71.8	22.00	0.35

[a] Rest-frame days since the estimated time of shock breakout on MJD 56396.5.
[b] AB magnitudes, not corrected for Galactic extinction, and with the host galaxy flux removed.

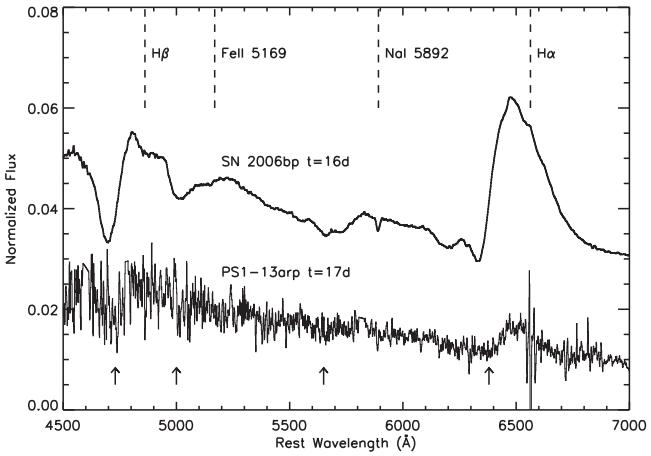

Figure 2. Gemini spectrum of PS1-13arp (smoothed by 2 pixels) at ∼17 rest-frame days since shock breakout, in comparison to SN 2006bp at 16 rest-frame days since shock breakout. Arrows show the potential P Cygni absorption features associated with broad $H\beta$, Fe IIλ5169, Na Iλ5892, and Hα, whose central wavelengths are marked with dashed lines.

spectrum by subtracting the 1D galaxy spectrum from the 1D SN+galaxy spectrum. We coadded the first two exposures, which had the highest SN signal. We show the coadded SN spectrum in Figure 2, in comparison to the spectrum of SN 2006bp at a similar phase since shock breakout from Quimby et al. (2007). We detect the P Cygni absorption features of Hβ, Fe II λ5169, Na Iλ5892, and Hα. We fit the strong broad Hα line with a Gaussian with an FWHM $= 7500 \pm 1200\,\mathrm{km\,s^{-1}}$ (shown in Figure 3). The line appears mostly symmetric, and blueshifted by $2200 \pm 100\,\mathrm{km\,s^{-1}}$ from the galaxy's narrow Hα line. We only see weak evidence of blueshifted absorption, as one would expect in a P Cygni profile. The weak blueward absorption is consistent with a young SN IIP, which typically do not develop a strong P Cygni Balmer line shape until ∼3 weeks after explosion (Quimby et al. 2007; Dessart et al. 2008). However, the weak P Cygni absorption could also reveal unusual conditions in the SN envelope or circumstellar environment. Unfortunately, without a later epoch of spectroscopy, we can only speculate as to whether PS1-13arp would have developed a stronger P Cygni line profile at late times.

3. COMPARISON TO SNe IIP

In Figure 4 we plot the *GALEX* NUV plus PS1 $g_{\rm P1}$, $r_{\rm P1}$, $i_{\rm P1}$, $z_{\rm P1}$ light curve of PS1-13arp. The global trends in the light curve are a ∼1 day NUV burst, a rapid $g_{\rm P1}$-band decline of ∼2.5 mag/(100 days), and an over 50 day plateau in the $g_{\rm P1}$ and $i_{\rm P1}$ bands. The optical light curve is characteristic of a normal SN IIP and is well fitted with the spectral synthesis model for SN IIP 2006bp (Dessart et al. 2008) *K*-corrected to a redshift similar to PS1-13arp (the model for SNLS-04D2dc at $z = 0.1854$ from Gezari et al. 2008; shown in Figure 4). The excellent agreement of the colors in the plateau implies a very small amount of internal extinction ($A_{\rm V} < 0.1$ mag). We applied a scaling of $\left(1 + z_{\rm 13arp}\right)$ in the time axis to account for time dilation, and we used a minimized χ^2 fit to the four optical bands to determine a vertical offset factor of -0.058 ± 0.036 applied to all bands, as well as a horizontal shift, inferring a time of shock breakout for PS1-13arp of MJD 56396.49 ± 0.40. This explosion time, determined entirely from the optical bands, is consistent with the timing of the NUV burst, and occurs 10 ± 8 rest-frame hours after the last NUV upper limit. It is also in excellent agreement with the time of explosion determined from Bayesian parametric model fitting to the optical light curve in Sanders et al. (2014) of MJD 56396.6 ± 0.5. The absolute magnitude of M_p, $r = -17.54 \pm 0.12$ mag of the *r*-band plateau at 50 days (Sanders et al. 2014) is 0.2 mag fainter than SN 2006bp, and well within the range of normal Type IIP luminosities.

We calculate the peak absolute magnitude of the NUV burst to be

$$M_{\rm NUV} = m - {\rm DM} - A_{\rm Gal} = -18.0\ {\rm mag},$$

where we use $m = 21.6$ mag, $d_{\rm L} = 800$ Mpc, DM = 39.5 mag, and Galactic extinction $A_{\rm Gal} = 8.2E(B-V) = 0.13$ mag, where $E(B-V) = 0.016$ mag. Note that for a hot blackbody temperature of $\approx 10^5$ K, the *GALEX* NUV effective wavelength, $\lambda_{\rm rest} = 2316\ \text{Å}/(1+z) = 1985$ Å, is on the Rayleigh–Jeans tail, and the *K* correction could be as large as $K(z) \approx -7.5 \log(1+z) = -0.5$ mag. The peak UV magnitude is consistent with theoretical predictions for the peak of shock breakout in an RSG (Gezari et al. 2008; Schawinski et al. 2008; Nakar & Sari 2010; Rabinak & Waxman 2011) and is brighter than the post-shock-breakout cooling peak that has definitively been observed in SNe IIP, SNLS-04D2ck with NUV = −17.0 mag (Gezari et al. 2008) and SN 2010aq with NUV = −17.3 mag (Gezari et al. 2010). In Figure 5 we show a comparison of UV light curves from *GALEX* for two SNe IIP caught rising in the UV, SN SNLS-04D2dc (Gezari et al. 2008) and SN 2010aq (Gezari et al. 2010). The comparison SNe have been offset in the vertical direction and corrected for time dilation. While the optical behavior of the SNe is quite similar, there is a clear excess again in the UV burst of PS1-13arp, implying a different source of energy from the cooling envelope model fitted successfully to these comparison SNe.

4. COMPARISON TO MODELS

4.1. Shock Breakout in the Stellar Envelope

While a burst of neutrinos marks the time of core collapse, the SN shock breakout is the first electromagnetic signature of an SN explosion. The SN shock "breaks out" when the radiative diffusion timescale,

$$t_{\rm d} \sim \frac{3(\delta R)^2}{\lambda c} = \frac{3\kappa\rho(\delta R)^2}{c} \approx \frac{3\tau H_\rho}{c},$$

where δR is the depth of the shock, $\lambda = 1/\kappa\rho$ is the photon's mean free path, κ is the opacity, τ is the optical depth, and H_ρ is the atmospheric scale height, is shorter than the shock travel time, $t_s = \delta R/v_s$ (Arnett 1996). For a standard RSG envelope density and radial structure, the duration of the radiative precursor is expected to be ∼1000 s (Klein & Chevalier 1978; Matzner & McKee 1999). However, the shock breakout pulse will be prolonged up to ∼1 hr due to light-travel time effects in the largest RSGs (Levesque et al. 2005), or up to days in the presence of a dense circumstellar wind (Ofek et al. 2010; Chevalier & Irwin 2011; Moriya et al. 2011).

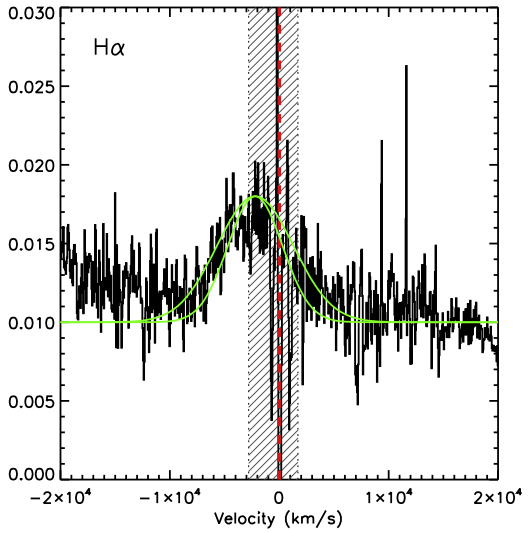

Figure 3. Hα profile of PS1-13arp at ∼17 rest-frame days since shock breakout. The line is broad (FWHM = 7500 ± 1200 km s^{-1}, Gaussian plotted with green lines) and blueshifted by 2200 ± 100 km s^{-1}. The red dashed line indicates zero velocity defined by the host galaxy Hα line. The hashed region indicates the location of the telluric A band feature that has been corrected for in the line profile. The profile is mostly symmetric, and does not yet demonstrate the strong P Cygni absorption that develops in SNe IIP typically three weeks after explosion.

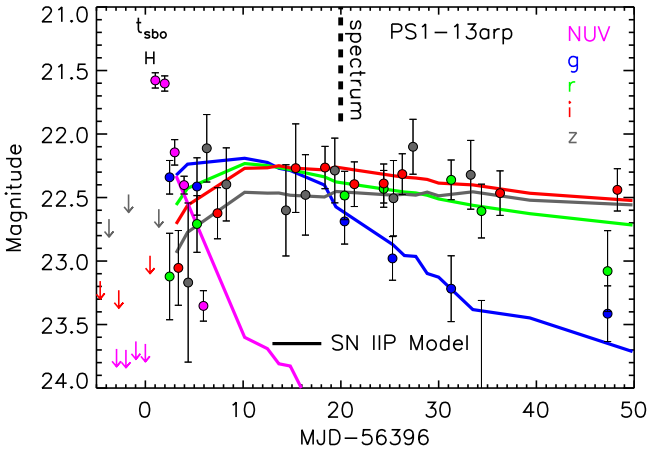

Figure 4. *GALEX* NUV and PS1 g_{P1},r_{P1},i_{P1},z_{P1} light curve of PS1-13arp with 1σ error bars and arrows indicating 3σ upper limits. The dotted magenta line traces the ∼1 day UV burst. The thick black line indicates the time of the Gemini GMOS-N spectrum. Thick solid lines show the CMFGEN model for SN 2006bp (modified to the rest frame of SNLS-04D2dc at $z = 0.1854$, close in redshift to PS1-13arp) in the NUV g, r, i, and z bands from Dessart et al. (2008) scaled by a factor of $\left(1 + z_{13arp}\right)$ in the time axis to account for time dilation. We use a minimized χ^2 fit to the four optical bands in order to determine the time of shock breakout (t_{sbo}) of MJD 56396.49 ± 0.40 in PS1-13arp, or 10±8 rest-frame hours after the last NUV non-detection, and a vertical offset that is applied to all bands of −0.058 ± 0.036 mag.

The rise time and duration of the UV burst in PS1-13arp are a factor of greater than ∼50 longer than both the radiative diffusion time at shock breakout from Matzner & McKee (1999),

$$t_{\rm sbo} = 860 k^{-0.58} (\rho_1/\rho_*)^{-0.28} E_{51}^{-0.79} M_{15}^{0.21} R_{500}^{2.16} \ {\rm s},$$

where R_{500} is the stellar radius in units of 500 $R_\odot$, M_{10} is the stellar mass in units of 10 $M_\odot$, and E_{51} is the energy of the explosion in units of 10^{51} erg s^{-1}, and the light-crossing time of an RSG,

$$t_{lc} = R_\star/c = 1160 R_{500} \ {\rm s}.$$

Even assuming an envelope density a factor of 1000 less dense than the standard stellar structure models of Woosley & Heger (2007), as was done in Schawinski et al. (2008), one can increase $t_{\rm sbo}$ only by a factor of ∼7. However, such an extended, tenuous structure is better attributed to a circumstellar shell of material rather than the stellar envelope itself (Falk & Arnett 1977). The long duration of the UV burst suggests that either the shock is "breaking out" in a wind around the progenitor star, or it is associated with the post-shock-breakout cooling envelope emission previously detected in the UV in SNe IIP with *GALEX* (Gezari et al. 2008, 2010; Schawinski et al. 2008; Ganot et al. 2014). In the following sections, we address both scenarios.

4.2. Cooling Envelope Emission

In the cooling envelope scenario, the *GALEX* observations did not catch the brief radiative precursor from shock breakout, but rather the UV burst is from the adiabatically expanding shock-heated SN ejecta. As the hot envelope expands and cools, the peak energy of the thermal emission shifts from the soft X-rays into the UV when $3kT = h\nu_{\rm NUV}(1+z)$, where $\nu_{\rm NUV} = 2316$ Å (or $T = 2.09$ eV), causing a peak in the NUV light curve. The rate of cooling depends sensitively on the radius of the progenitor, since the smaller the progenitor, the more energy is lost to adiabatic expansion. Using the analytical model for the cooling envelope emission for an RSG, the largest likely SN II progenitor, from Nakar & Sari (2010), this occurs at a time

$$t_{\rm peak,NUV} = 1.9 \, M_{15}^{-0.23} R_{500}^{0.68} E_{51}^{0.20} {\rm days}.$$

The rise time in PS1-13arp is constrained from the time between the last NUV non-detection and the first NUV detection to be <0.87 days in the SN rest frame, or from the fitted time of shock breakout from Section 3 to be <0.5 ± 0.3 days. In order for this UV rise time to be compatible with PS1-13arp, it would require $M_{15}^{-0.23} R_{500}^{0.68} E_{51}^{0.20} < 0.46$. The UV peak can occur much sooner for a smaller star, such as a BSG ($t_{\rm peak} \approx 0.54$ days). However, the late-time optical light curve of PS1-13arp is incompatible with such a compact progenitor. For a BSG with a typical radius of a factor of 10 smaller than an RSG, one would expect a redder and shorter-duration plateau (Kleiser et al. 2011; Dessart et al. 2013), which is inconsistent with the excellent fit of the plateau of SN PS-13arp to the SN 2006bp model.

Figure 6 shows the evolution of the UV/optical spectral SED of PS1-13arp over time, with NUV fluxes linearly interpolated to the time of the PS1 observations. Unfortunately, we do not have a strong constraint on the temperature of the UV burst. We can only apply a lower limit from the z-band non-detection of $T > 2.2 \times 10^4$ K. Given that the next epoch, at a phase (ϕ) of 1.7 rest-frame days since our estimated time of shock breakout, is hotter, with a least-squares fitted temperature of $T = (2.8 \pm 0.3) \times 10^4$ K, we adopt this as our lower limit to the temperature of the UV burst at $\phi = 0.8$ days, since the SN should be cooling with time. The NUV flux density, corrected for Galactic extinction, then corresponds to a peak bolometric

luminosity of $L_{\rm bol} > 1.7 \times 10^{43}$ erg s^{-1}, which is an order of magnitude larger than expected for the cooling envelope at the time of the NUV peak from Nakar & Sari (2010):

$$L_{\rm RSG,peak} = 2.70 \times 10^{42} M_{15}^{-0.87} R_{500} E_{51}^{0.96} {\rm erg\ s^{-1}}.$$

The observed NUV absolute magnitude of PS1-13arp is also brighter than the corresponding peak absolute magnitude of this model of $M_{\rm NUV} \sim -16$ mag. For a BSG, the luminosity at the time of the NUV peak is even lower ($L_{\rm BSG,peak} \sim 8 \times 10^{41}$ erg s^{-1}). Figure 7 compares the early UV/optical light curve of PS1-13arp with the RSG SN shock breakout and cooling envelope emission model from Nakar & Sari (2010), scaled to match the late-time SN 2006bp model fit. While the observations and model are in good agreement close to the cooling envelope model peak and later ($t > 2$ days), there is a clear prolonged UV excess above the model at earlier times. We conclude that the peak of the observed UV burst is more luminous than expected for the cooling envelope emission following shock breakout, and thus we now investigate whether or not the UV burst could be from the shock breakout pulse itself but prolonged in time due to the presence of a circumstellar wind.

4.3. Shock Breakout in a Circumstellar Wind

The "shock breakout" is defined as when the radiation from the SN shock is able to escape in front of the shock, i.e., when the radiative diffusion time is shorter than the shock travel time (see Section 4.1). For a bare star, this occurs in the outer envelope of the star (not actually at its surface). However, when the star is enshrouded in a dense wind, the shock breakout is delayed and occurs outside the surface of the star in the circumstellar wind. The theoretical literature still refers to this phenomenon as the shock breakout (Balberg & Loeb 2011; Chevalier & Irwin 2011; Ofek et al. 2013), even though the energy deposited from the shock is diffusing out (escaping) into the wind instead of the stellar envelope. A radiation-dominated shock in a uniform medium has a characteristic thickness in units of optical depth of $\tau_s \approx c/v_s$. The shock will breakout in the wind if $\tau_w > \tau_s$, where τ_w is the thickness of the shock traveling through the wind in units of optical depth. Here we assume the wind is from steady mass loss from the progenitor star $\dot{M}$, resulting in a density distribution $\rho_w = \dot{M}/4\pi r^2 v_w \equiv Dr^{-2}$, where $D \equiv 5.0 \times 10^{16} \left(\dot{M}_{0.01}/v_{w,10}\right)$ g cm^{-1} and $\dot{M}_{0.01} = \dot{M}/(0.01 M_\odot\ {\rm yr}^{-1})$, and we assume the slow wind velocity characteristic of an RSG, $v_{w,10} = v_w/(10\ {\rm km\ s^{-1}})$. Chevalier & Irwin (2011) approximate the optical depth of a shock wave traveling through the wind as $\tau_w \approx R_d^{-1} \kappa D$, where R_d is the depth of the shock. Hence, shock breakout occurs when $\tau_w \approx c/v_s$, such that $R_d = \kappa D v_s/c$. The luminosity of the breakout radiation is given by $L_{\rm bo} \approx E_{\rm rad}/t_{\rm bo}$, where $E_{\rm rad}$ is the radiative energy in the breakout shell and $t_{\rm bo} = R_d/v_s = \kappa D/c = 6.6k\left(\dot{M}_{0.01}/v_{w,10}\right)$ days, where $t_{\rm bo}$ is the time of shock breakout and $k = \kappa/(0.34\ {\rm cm^2\ g^{-1}})$. This is given in Chevalier & Irwin (2011) as $L_{\rm bo} \approx E_{\rm rad}/t_{\rm bo}$, and thus

$$L_{\rm bo} = 6.0 \times 10^{43} k^{-0.6} E_{51}^{1.2} M_{15}^{-0.6} \left(\dot{M}_{0.01}/v_{w,10}\right)^{-0.2} {\rm erg\ s^{-1}},$$

with a corresponding temperature of

$$T_{\rm rad} = 1.1 \times 10^5 k^{-0.25} \left(t_{d,1}\right)^{-0.25} K,$$

where $t_{d,1} = t_d/(1\ {\rm day})$. Given the observed rise time of $t_{\rm rise} \lesssim 0.87$ days in the SN rest frame and the weak dependence of T on t_d, we assume a shock breakout radiation temperature of

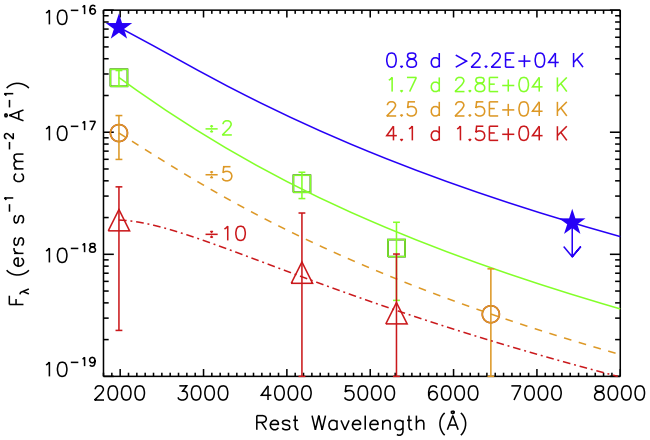

Figure 6. Interpolated spectral energy distributions (SEDs) of PS1-13arp with time and their least-squares fitted blackbody temperatures. The time of each epoch is labeled in rest-frame days since the estimated time of shock breakout of MJD 56396.5 from Figure 4. The temperature of the earliest epoch is constrained by a z-band upper limit to be $T > 2.2 \times 10^4$ K. The SEDs for 1.7, 2.5, and 4.1 days have been divided by factors of 2, 5, and 10, respectively, for clarity.

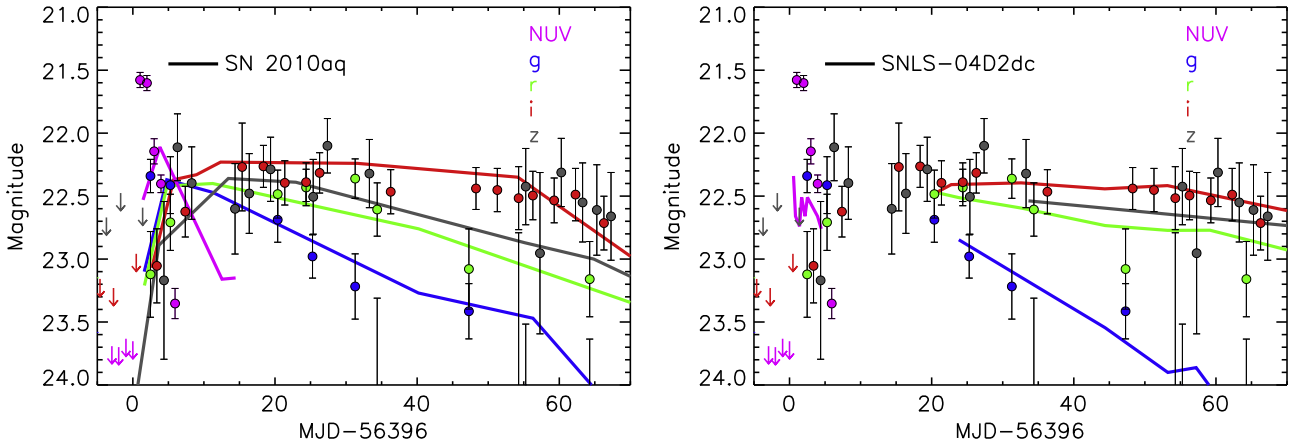

Figure 5. SNe II with early UV photometry. Comparison with SN 2010aq (left) and SNLS-04D2dc (right). A constant offset of +1.47 mag has been applied to the SN 2010aq data from Gezari et al. (2010) and –0.27 mag to SNLS-04D2dc data from Gezari et al. (2008), plotted with solid thick lines. For clarity, we do not plot the *GALEX* FUV light curve of SNLS-04D2dc, which has a lower signal-to-noise ratio than the NUV light curve.

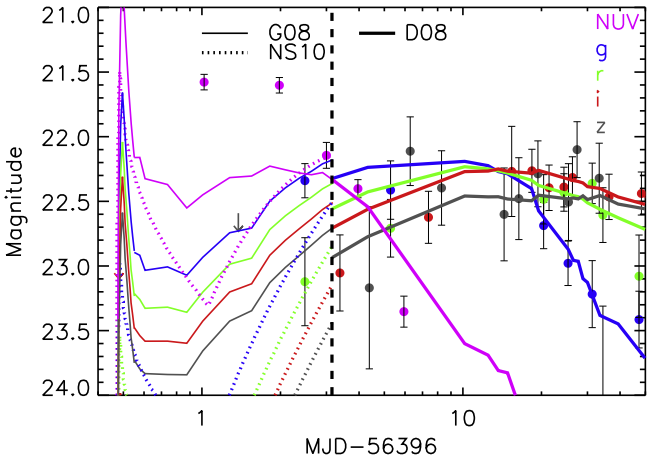

Figure 7. Light curve of PS1-13arp on a logarithmic timescale to compare the early UV emission to models for shock breakout and the cooling envelope in more detail. Thick lines show the SN IIP model from Dessart et al. (2008) fitted to PS1-13arp in Figure 4; thin solid lines show the numerical model for shock breakout from the stellar surface and its cooling envelope from Gezari et al. (2008, G08) for an RSG with $R = 865R_{\odot}$, $M = 12.58M_{\odot}$, and $E = 1.2 \times 10^{51}$ erg; and dotted lines show the analytical surface shock breakout and cooling envelope model from Nakar & Sari (2010, NS10) for $R = 500R_{\odot}$, $M = 15M_{\odot}$, and $E = 1 \times 10^{51}$ erg. The G08 model has been shifted vertically to overlap with the D08 model fit to PS1-13arp at $t > 3$ days in the NUV. The NS10 model has been shifted vertically to match the NUV data point for PS1-13Rp at $t \sim 3$ days. Note the clear excess in the observed NUV emission above the cooling envelope emission components for both models at $t \sim 1 - 2$ days.

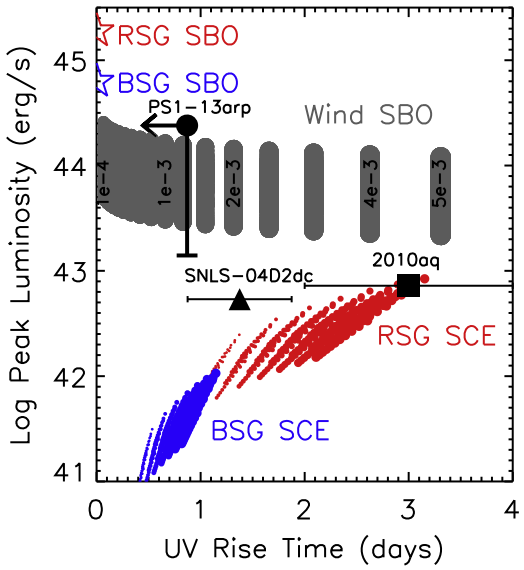

Figure 8. Parameter space of peak bolometric luminosity vs. the rise time to peak in the NUV covered by models for shock breakout in the stellar envelope for an RSG (red star) and BSG (blue star), shock breakout into a wind (gray bars), and the shock cooling envelope for a BSG (blue dots) and RSG (red dots) with a range of values for $\dot{M}$, R, M, and E. The sizes of the dots are scaled by the relative size of R within the range of values of 250−850 $R_{\odot}$ for RSGs and 25–85 $R_{\odot}$ for BSGs. The ranges of the other SN parameters are $M = 10 - 25\ M_{\odot}$, $E = (0.5-1.5) \times 10^{51}$ erg. The wind mass-loss rate range is $\dot{M} = (.01-5) \times 10^{-3}\ M_{\odot}\ \mathrm{yr}^{-1}$, with some values labeled on the diagram. The peak bolometric luminosity and UV rise time are plotted for PS1-13arp (black dot), SN 2010aq (black square), and SN SNLS-04D2dc (black triangle). The peak bolometric luminosity of PS1-13arp is plotted ranging from a lower limit for the observed SED with $T > 2.8 \times 10^4$ K up to the expected wind shock breakout model temperature of $T \approx 10^5$ K.

$T \approx 10^5$ K, which is allowed by our observed SED at the UV peak based on the z-band upper limit during the UV burst. Given our observed Galactic-extinction corrected luminosity density in the NUV of $L_{\nu_e=(1+z)\nu_o} = f_{\nu_o} 4\pi d_{\mathrm{L}}^2/(1+z) = 6.25 \times 10^{27}$ erg s^{-1} Hz^{-1} and assuming radiation from an optically thick blackbody, for which $L_{\nu} = \left(2\pi h/c^2\right)\nu^3/\left(e^{h\nu/kT} - 1\right)4\pi R_{\mathrm{bb}}^2$, one gets $R_{\mathrm{bb}} = 5.8 \times 10^{13}$ cm and a bolometric luminosity of 2.4×10^{44} erg s^{-1} (a factor of 14 greater than the observed lower limit). The inferred radius is close to the upper range of radii measured for RSGs ($2-6 \times 10^{13}$ cm; Levesque et al. 2005) and is potentially situated *outside* the stellar envelope in the circumstellar wind. Given the rise time of $\lesssim$0.87 days, this radius then corresponds to a shock velocity of $v_s \gtrsim 7 \times 10^3$ km s^{-1}, similar to the velocity width of the detected broad Hα line.

The Chevalier & Irwin (2011) model places two independent constraints on the mass-loss rate ($\dot{M}$). The first is from the timescale of the event. The observed rise time corresponds to $\dot{M} \lesssim 1.3 \times 10^{-3}\left(v_{w,10}/k\right)t_{d,1}M_{\odot}$ yr^{-1}. The duration of the shock breakout signal in the Chevalier & Irwin (2011) wind model is on the order of the rise time to peak. Thus, the rise time in PS1-13arp cannot be much shorter than the duration of the UV burst of $\gtrsim$0.82 days in the SN rest frame. Thus, we favor a mass-loss rate closer to $10^{-3}\,M_{\odot}$ yr^{-1}. The observed luminosity corresponds to $\dot{M} \sim 1 \times 10^{-5}(v_{w,10})k^{-3}E_{51}^6 M_{15}^{-3}\ M_{\odot}$ yr^{-1}. Given the strong sensitivity of the peak luminosity to E_{51}, this could be easily reconciled with the mass-loss rate estimated from the timing of the event by adopting an explosion energy of $E_{51} \sim 1.5$. Figure 8 plots the parameter space for peak bolometric luminosity versus rise time to peak in the NUV for shock breakout in a wind and cooling envelope emission for BSGs and RSGs with a range of $E_{51} = (0.5-1.5) \times 10^{51}$ erg, $R = 250-850\ R_{\odot}$ for the RSG and $R = 25-85$ for the BSG, and $M = 10-25\ M_{\odot}$. The observed peak luminosity of PS1-13arp is well above that expected for the cooling envelope phase, and is within the range of luminosities and timescales for a burst powered by shock breakout in a wind.

The upper limit on $\dot{M}$ from the observed rise time is consistent with the lack of excess thermal radiation in the optical bands at later times. Moriya et al. (2011) model the light curves of SNe IIP as a function of $\dot{M}$, and find that for $\dot{M} > 10^{-3}M_{\odot}$ yr^{-1} there is an observable excess in the UV and optical bands due to the conversion of the kinetic energy of the ejecta into thermal energy via interaction with the CSM. The mass-loss rates in RSGs inferred from spectroscopic studies range from 10^{-7} to $10^{-4}\dot{M}$ yr^{-1} (van Loon et al. 2005; Mauron & Josselin 2011). Thus, while the inferred mass-loss rate from the luminosity and duration of the shock breakout is on the high end of the observed distribution, these studies are sensitive to the time-averaged mass-loss rate and do not sample short-lived, episodic enhanced mass-loss that may occur in pre-supernova RSGs (Meynet et al. 2014), perhaps as a result of pulsation-driven superwinds (Yoon & Cantiello 2010). Unfortunately, we do not have a sufficient signal-to-noise ratio (S/N) in the spectrum of PS1-13arp to look for a high-velocity absorption feature or "notch," predicted to be a signature of the excitation of ejecta by X-rays produced by circumstellar interaction (Chugai et al. 2007).

X-ray and radio observations of SNe IIP also put conservative upper limits on the mass-loss rates of pre-SN RSGs to $<10^{-6}-10^{-5}\,M_{\odot}$ yr^{-1} from the lack of thermal bremsstrahlung emission or synchrotron radiation from the interaction of the SN shock wave with the CSM (Chevalier et al. 2006; Dwarkadas 2014). Radio and X-ray emission from SN IIP 1999em were interpreted as the result of circumstellar interaction with a stellar wind of $\dot{M} \sim 2 \times 10^{-6}\,M_{\odot}$ yr^{-1} (Pooley et al. 2002). Mass-loss rates should scale with the RSG luminosity, and thus with stellar mass. Sanders et al. (2014) were not able to put a direct constraint on the progenitor mass of PS1-13arp from the comparison of the bolometric light curve to hydrodynamic models; however, they did infer an ejected nickel mass from a comparison of the late-time bolometric light curve of PS1-13arp to SN 1987 A of $M_{\rm Ni} = 0.34^{+0.20}_{-0.22} M_{\odot}$. This amount of nickel is on the high-mass tail of the distribution for their SNe IIP sample, and could be indicative of a more massive progenitor RSG for PS1-13arp. Another clue is the weak P Cygni absorption in the Hα profile of PS1-13arp at $t \sim 17$ days. Weak P Cygni absorption has been found in brighter than normal SNe IIP and is explained by lower envelope masses and higher mass-loss rates (Gutiérrez et al. 2014).

5. CONCLUSIONS

We present the joint *GALEX* UV and PS1 optical discovery of an SN IIP with a normal optical light curve, including the trademark plateau, preceded by a UV burst with a peak luminosity expected from shock breakout, but with a longer than expected duration. We rule out shock cooling emission from a compact BSG progenitor, and favor a shock breakout from an RSG with a high, but not extreme, amount of pre-SN mass loss ($\approx 10^{-3}\,M_{\odot}$ yr^{-1}). This mass-loss rate is high enough to increase the height at which the SN shock breaks out to beyond the stellar surface, but not large enough to affect the optical light curve or spectrum measured weeks after the explosion. In particular, we do not detect narrow emission lines that could be powered by interaction with a dense CSM (from $\dot{M} \sim 0.01\,M_{\odot}$ yr^{-1} to $0.1\,M_{\odot}$ yr^{-1}) as seen in SNe IIn (Turatto et al. 1993; Chugai & Danziger 1994; Smith et al. 2008).

However, we must caution that the theoretical models discussed here have yet to be verified in the normal case of shock breakout in the stellar envelope. In the case of SN IIP SNLS-04D2dc, the early *GALEX* UV photometry could be fitted either with a delayed shock breakout in a non-standard, extended, low-density envelope of an RSG followed by the cooling envelope (Schawinski et al. 2008), or a numerical simulation for only the cooling envelope component (Gezari et al. 2008). The cadence (~1.5 hr) and low S/N photometry (S/N ~ 2–4) in this source were not enough to favor one model over the other, let alone constrain their detailed parameters. While a wind effectively smears out the shock breakout signal and makes it possible to resolve with a coarser (one-day) cadence, as we report here for PS1-13arp, this interpretation would have stronger footing if the theory were proven in the more common case of shock breakout in the SN envelope.

Rapid-cadence observations on a timescale of minutes, particularly in the UV band, are required to resolve the putative rapid rise from shock breakout in the SN light curve and its second UV peak due to the cooling envelope. Future observations of shock breakout of SNe IIP in the UV could be a sensitive probe of the mass-loss history of pre-SN RSGs, which is difficult to constrain directly (Meynet et al. 2014). Furthermore, the presence of a wind will greatly enhance the ability of future UV time domain surveys, such as ULTRASAT (Sagiv et al. 2014), to directly detect this diagnostic phase of the SN explosion.

S.G. thanks the Gemini Deputy Director for approving a change of program for the TOO program GN-2013A-Q-32 to observe PS1-13arp. The Pan-STARRS1 Surveys (PS1) have been made possible through contributions of the Institute for Astronomy, the University of Hawaii, the Pan-STARRS Project Office, the Max Planck Society and its participating institutes, the Max Planck Institute for Astronomy, Heidelberg, and the Max Planck Institute for Extraterrestrial Physics, Garching, The Johns Hopkins University, Durham University, the University of Edinburgh, Queen's University Belfast, the Harvard-Smithsonian Center for Astrophysics, the Las Cumbres Observatory Global Telescope Network Incorporated, the National Central University of Taiwan, the Space Telescope Science Institute, the National Aeronautics and Space Administration under grant No. NNX08AR22G issued through the Planetary Science Division of the NASA Science Mission Directorate, the National Science Foundation under grant No. AST-1238877, the University of Maryland, and Eotvos Lorand University (ELTE).

REFERENCES

Abazajian, K. N., Adelman-McCarthy, J. K., Agüeros, M. A., et al. 2009, ApJS, 182, 543
Arnett, D. 1996, Supernovae and Nucleosynthesis
Balberg, S., & Loeb, A. 2011, MNRAS, 414, 1715
Becker, A. C., Wittman, D. M., Boeshaar, P. C., et al. 2004, ApJ, 611, 418
Berger, E., Chornock, R., Lunnan, R., et al. 2012, ApJL, 755, L29
Blinnikov, S. I., Nadyozhin, D. K., Woosley, S. E., & Sorokina, E. I. 2002, in Nuclear Astrophysics, ed. W. Hillebrandt & E. Müller (Garching: Max Planck Inst. für Astrophysik), 144
Chevalier, R. A., Fransson, C., & Nymark, T. K. 2006, ApJ, 641, 1029
Chevalier, R. A., & Irwin, C. M. 2011, ApJL, 729, L6
Chomiuk, L., Chornock, R., Soderberg, A. M., et al. 2011, ApJ, 743, 114
Chugai, N. N., Chevalier, R. A., & Utrobin, V. P. 2007, ApJ, 662, 1136
Chugai, N. N., & Danziger, I. J. 1994, MNRAS, 268, 173
Dessart, L., Hillier, D. J., Waldman, R., & Livne, E. 2013, MNRAS, 433, 1745
Dessart, L., Blondin, S., Brown, P. J., et al. 2008, ApJ, 675, 644
Drout, M. R., Chornock, R., Soderberg, A. M., et al. 2014, ApJ, 794, 23
Dwarkadas, V. V. 2014, MNRAS, 440, 1917
Ensman, L., & Burrows, A. 1992, ApJ, 393, 742
Falk, S. W. 1978, ApJL, 225, L133
Falk, S. W., & Arnett, W. D. 1977, ApJS, 33, 515
Ganot, N., Gal-Yam, A., Ofek, E. O., et al. 2014, arXiv:1412.4063
Gezari, S., Dessart, L., Basa, S., et al. 2008, ApJL, 683, L131
Gezari, S., Martin, D. C., Forster, K., et al. 2013, ApJ, 766, 60
Gezari, S., Rest, A., Huber, M. E., et al. 2010, ApJL, 720, L77
Gutiérrez, C. P., Anderson, J. P., Hamuy, M., et al. 2014, ApJL, 786, L15
Hamuy, M., Suntzeff, N. B., Gonzalez, R., & Martin, G. 1988, AJ, 95, 63
Heger, A., Fryer, C. L., Woosley, S. E., Langer, N., & Hartmann, D. H. 2003, ApJ, 591, 288
Hodapp, K. W., Siegmund, W. A., Kaiser, N., et al. 2004, in SPIE Conf. Ser. 5489, Ground-based Telescopes, ed. J. M. Oschmann, Jr., 667
Kaiser, N., Burgett, W., Chambers, K., et al. 2010, in SPIE Conf. Ser. 77330
Kewley, L. J., & Dopita, M. A. 2002, ApJS, 142, 35
Klein, R. I., & Chevalier, R. A. 1978, ApJL, 223, L109
Kleiser, I. K. W., Poznanski, D., Kasen, D., et al. 2011, MNRAS, 415, 372
Levesque, E. M., Massey, P., Olsen, K. A. G., et al. 2005, ApJ, 628, 973
Lunnan, R., Chornock, R., Berger, E., et al. 2013, ApJ, 771, 97
Magnier, E. 2006, in Proc. Advanced Maui Optical and Space Surveillance Technologies Conf., ed. S. Ryan (Maui, HI: The Maui Economic Development Board), E50

Magnier, E. 2007, in ASP Conf. Ser. 364, The Future of Photometric, Spectrophotometric and Polarimetric Standardization, ed. C. Sterken (San Francisco, CA: ASP), 153
Magnier, E. A., Liu, M., Monet, D. G., & Chambers, K. C. 2008, in IAU Symp. 248, ed. W. J. Jin, I. Platais, & M. A. C. Perryman (Cambridge: Cambridge Univ. Press), 553
Martin, D. C., Fanson, J., Schiminovich, D., et al. 2005, ApJL, 619, L1
Matzner, C. D., & McKee, C. F. 1999, ApJ, 510, 379
Mauron, N., & Josselin, E. 2011, A&A, 526, A156
Meynet, G., Chomienne, V., Ekström, S., et al. 2014, arXiv:1410.8721
Modjaz, M., Li, W., Butler, N., et al. 2009, ApJ, 702, 226
Moriya, T., Tominaga, N., Blinnikov, S. I., Baklanov, P. V., & Sorokina, E. I. 2011, MNRAS, 415, 199
Morrissey, P., Conrow, T., Barlow, T. A., et al. 2007, ApJS, 173, 682
Nakar, E., & Sari, R. 2010, ApJ, 725, 904
Noll, S., Burgarella, D., Giovannoli, E., et al. 2009, A&A, 507, 1793
Ofek, E. O., Fox, D., Cenko, S. B., et al. 2013, ApJ, 763, 42
Ofek, E. O., Rabinak, I., Neill, J. D., et al. 2010, ApJ, 724, 1396
Pooley, D., Lewin, W. H. G., Fox, D. W., et al. 2002, ApJ, 572, 932
Quimby, R. M., Wheeler, J. C., Höflich, P., et al. 2007, ApJ, 666, 1093
Rabinak, I., & Waxman, E. 2011, ApJ, 728, 63
Rest, A., Scolnic, D., Foley, R. J., et al. 2014, ApJ, 795, 44
Rest, A., Stubbs, C., Becker, A. C., et al. 2005, ApJ, 634, 1103
Sagiv, I., Gal-Yam, A., Ofek, E. O., et al. 2014, AJ, 147, 79
Sanders, N. E., Soderberg, A. M., Gezari, S., et al. 2014, arXiv:1404.2004
Schawinski, K., Justham, S., Wolf, C., et al. 2008, Sci, 321, 223
Schechter, P. L., Mateo, M., & Saha, A. 1993, PASP, 105, 1342
Smartt, S. J., Eldridge, J. J., Crockett, R. M., & Maund, J. R. 2009, MNRAS, 395, 1409
Smith, N., Chornock, R., Li, W., et al. 2008, ApJ, 686, 467
Soderberg, A. M., Berger, E., Page, K. L., et al. 2008, Natur, 453, 469
Stetson, P. B. 1987, PASP, 99, 191
Stritzinger, M., Hamuy, M., Suntzeff, N. B., et al. 2002, AJ, 124, 2100
Stubbs, C. W., Doherty, P., Cramer, C., et al. 2010, ApJS, 191, 376
Svirski, G., & Nakar, E. 2014, ApJL, 788, L14
Tonry, J., & Onaka, P. 2009, in Advanced Maui Optical and Space Surveillance Technologies Conf., ed. S. Ryan (Kihei, HI: The Maui Economic Developer Board), E40
Tonry, J. L., Stubbs, C. W., Lykke, K. R., et al. 2012, ApJ, 750, 99
Tremonti, C. A., Heckman, T. M., Kauffmann, G., et al. 2004, ApJ, 613, 898
Turatto, M., Cappellaro, E., Danziger, I. J., et al. 1993, MNRAS, 262, 128
van Loon, J. T., Cioni, M.-R. L., Zijlstra, A. A., & Loup, C. 2005, A&A, 438, 273
Woosley, S. E., & Heger, A. 2007, Phys. Rep., 442, 269
Wright, E. L., Eisenhardt, P. R. M., Mainzer, A. K., et al. 2010, AJ, 140, 1868
Yoon, S.-C., & Cantiello, M. 2010, ApJL, 717, L62